



Unzipping polymers significantly enhance energy flux of aluminized composites

Haiyang Wang^a, Yujie Wang^a, Mayank Garg^{b,c}, Jeffrey S. Moore^{b,d}, Michael R. Zachariah^{a,*}

^a Department of Chemical and Environmental Engineering, The University of California, Riverside, CA 92521, USA

^b Beckman Institute for Advanced Science and Technology, University of Illinois at Urbana-Champaign, Urbana, Illinois 61801, USA

^c Department of Materials Science and Engineering, University of Illinois at Urbana-Champaign, Urbana, Illinois 61801, USA

^d Department of Chemistry, The University of Illinois Urbana-Champaign, Champaign, IL 61820, USA



ARTICLE INFO

Article history:

Received 19 October 2021

Revised 2 June 2022

Accepted 3 June 2022

Keywords:

Unzipping polymers

3D printing

Nanothermites

Energetic materials

High loading

ABSTRACT

This paper describes a new approach to enhancing the energy delivery rate of pyrotechnics by employing an unzipping polymer. The basic strategy is to localize the heat feedback to just near the reaction front by driving the endothermic chemistry of unzipping. This should then liberate gas near the flame front and propel particles away from the burning surface, to minimize agglomeration and sintering. In this study, polypropylene carbonate (PPC) is employed to load 90 wt% Al and CuO nanoparticles (NPs) via direct ink-writing. The results show a >1500% faster energy release rate from the aluminothermic reaction compared to a conventional polymer binder. Through in-operando microscopy, we observed a 6X thinner flame front and smaller combustion products, revealing significantly lower agglomeration of Al NPs with the unzipping polymer. Fast-heating Time-of-Flight Mass Spectrometry confirms that the unzipping polymer decomposes to low-molecular-weight gases at a relatively low temperature, which significantly reduces the sintering of Al NPs. The thinner flame implies that heat feedback to the unreacted materials is more localized and drives the endothermic unzipping reaction for gas generation. This study provides a new approach to substantially increasing the energy release rate of nanoscale metallic fuels.

© 2022 Published by Elsevier Inc. on behalf of The Combustion Institute.

1. Introduction

Metal fuels such as aluminum (Al) have energy densities of ≈ 30 kJ/g (≈ 80 kJ/cm³) with O₂, which is >3X higher than the most powerful explosives such as hexanitrohexaazaisowurtzitane (CL-20) [1,2]. For this reason, Al particles are commonly employed as additives in various energetic materials such as propellants, explosives, and pyrotechnics [3–10]. Nanoscale metallic fuels have been shown to be as much as 1000x more reactive than their micron-sized counterparts due to their high surface area to volume ratio. Unfortunately, significant sintering occurs on a time scale often shorter than the combustion time, which transforms the initial nanoscale fuel into microscale particles. This increase in particle size effectively slows down the energy release rate and mitigates some of the advantages of employing nanoscale metals [1–15].

To mitigate this problem, one strategy has been to preassemble the nanocomponents into larger microparticles, containing a gas generator triggered to react at temperatures below the ignition temperature of the metallic fuel. The gas generator ejects and

separates the individual NPs to reduce sintering and coalescence [14,15]. While this approach has shown considerable promise, it requires subsequent processing to create free-standing structures by assembling the microparticles with additional polymer binders [16–23].

Here, we describe a new approach that utilizes a chain-unzipping polymer (polypropylene carbonate, PPC) as a binder for energetic composite. PPC decomposes primarily through sequential monomer depolymerization [24]. The basic strategy is to localize the heat feedback to just near the reaction front by driving the endothermic chemistry of unzipping. This should then liberate gas near the flame front and propel particles away from the burning surface, to minimize agglomeration and sintering. The basic concept is illustrated in Fig. 1.

2. Experimental section

2.1. Chemicals

Hydroxypropyl methylcellulose (HPMC, brand name: METHOCEL™ F4M) has a molecular weight (M_w) of 86 kDa and a viscosity of 4000 cP (2% solution, 25 °C). Polyvinylidene fluoride (PVDF, M_w 534 kDa) and N, N-Dimethylformamide (DMF,

* Corresponding author.

E-mail addresses: mrz@engr.ucr.edu, mrz@umd.edu (M.R. Zachariah).

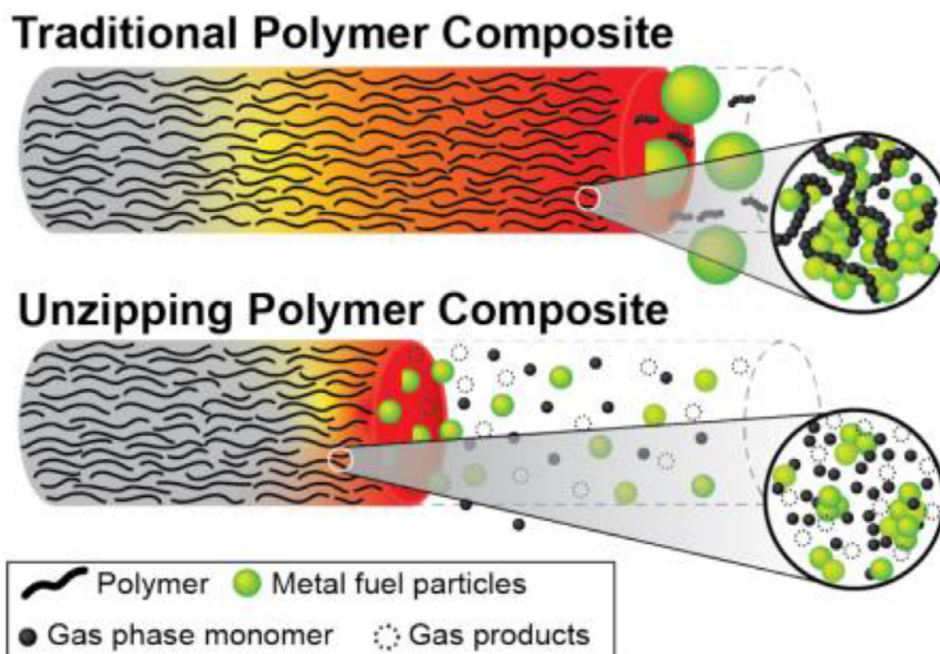


Fig. 1. Conceptualization of unzipping vs traditional polymer binder: Unzipping results in increased gas-phase products near the front leads to less particle sintering, promoting a higher burn rate and a narrower reaction front with smaller agglomerations compared to traditional polymer composite. (For interpretation of the references to colour in this figure legend, the reader is referred to the web version of this article.)

99.8%) were purchased from Sigma-Aldrich. Poly(propylene carbonate) (PPC) pellets ($M_w \approx 196$ kDa) were gifted by Novomer. 4-Methylphenyl [4-(1-methylethyl) phenyl] iodonium tetrakis (pentafluorophenyl) borate photoacid generator (PAG) catalyst, commercially known as Rhodorsil-FABA, was supplied by Bluestar Silicones [25]. CuO nanoparticles (≈ 40 nm) were purchased from US Research Nanomaterials. Aluminum nanoparticles (Al NPs, ≈ 50 nm) have an active content is ≈ 67 wt.% according to thermogravimetric/differential scanning calorimetry (TG/DSC) results.

2.2. Ink preparation

To prepare a stable ink for direct writing, 100 mg HPMC/PVDF (1:1 by mass) or PPC (with or without 1% PAG) was separately weighed and dissolved in 3.2 mL DMF and magnetically stirred for ≈ 2 hrs to get a clear solution [17,25]. Then 668.6 mg CuO and 231.4 mg Al NPs were dispersed into the above polymer solution by ultrasonication for ≈ 1 hr. Then the resulting slurry was magnetically and mechanically stirred for 24 hrs and 1 hr, respectively.

2.3. T-Jump ignition and mass spectrum

Details of the T-Jump ignition and mass spectrum are found in our previous study [26]. The above-mentioned polymer inks with and without Al/CuO nanothermite were characterized by our T-Jump ignition and mass spectrum system, respectively. Ignition of Al/CuO composites and decomposition of polymers were conducted in argon and vacuum, respectively, to get the ignition temperatures and decomposition species. Typically, the inks were coated and dried on a ≈ 10 mm long platinum filament (≈ 76 μm in diameter), which was resistively heated to ≈ 1400 K at a heating rate of $\approx 4 \times 10^5$ K·s $^{-1}$ (in 1 atm argon or in vacuum). The temporal filament resistance (correlated via the Callendar-Van Dusen Equation) during the heating process was recorded. The ignition and subsequent combustion of the composites were monitored using a high-speed camera (Phantom V12.1), and the ignition temper-

atures are obtained by coupling the observed ignition timestamp from the high-speed video with the filament temperature.

2.4. Direct-ink-Writing process

The obtained inks were extruded through an 18-gauge needle (inner diameter: 0.038" (≈ 0.96 mm)) at a feed rate of ≈ 9 mL/h and a printing speed (moving speed of the nozzle) of ≈ 25 cm/min. The substrate was kept at ≈ 75 °C to ensure removal of DMF and drying of the printing layer before depositing another layer. After printing, the samples were left on the heated substrate (kept at ≈ 75 °C) for another 30 mins to further evaporate any remaining solvent. The free-standing composite sticks were printed in 15 layers with a square of 8 cm \times 8 cm and were cut into 3 cm long sticks for combustion characterization. The density and porosity are determined by the mass divided by the volume (cross-sectional area \times length) of each stick. The porosity of the samples was estimated by $(1 - (\text{actual density}/\text{theoretical density}))$. Al/CuO composites were also printed on the glass slides with 3 layers for microscopic imaging of the flame front [17,25].

2.5. Morphology characterization

The microstructure of the printed samples was investigated by using a Thermo-Fisher Scientific NNS450 scanning electron microscope (SEM) coupled with energy-dispersive X-ray spectroscopy (EDS).

2.6. Macroscopic and microscopic imaging

All the combustion tests were conducted in argon (1 atm). As shown in Fig. S6, the samples are either free-standing burn sticks (≈ 1.5 cm long, for both macroscopic and microscopic imaging) or composites on glass slides (≈ 2.2 cm long, for microscopic imaging only). The sticks or glass slides were attached to steel support using a double-sided tape, and the support is mounted to a

3D translational stage for focus purposes. The macroscopic imaging high-speed camera (Vision Research Phantom Miro M110) has a resolution of $\approx 80 \mu\text{m}/\text{pixel}$ while the microscopic imaging system (Vision Research Phantom VEO710L coupled to Infinity Photo-Optical Model K2 DistaMax) has a resolution of $\approx 2 \mu\text{m}/\text{pixel}$.

2.7. Burn rate and flame temperatures

The linear burn rate (ν) and average flame temperature (T_{flame}) of the composite sticks were determined from the macroscopic videos. The samples were ignited by nichrome wire. Before reaching a steady state, <1 mm of sample is consumed. The linear burn rate was calculated by dividing the length of the sample by the total burning time. The energy release rate considers densities (ρ), burn rates (ν) and flame temperatures (energy release rate $\sim \rho \times \nu \times T$) [27,28] and is normalized to the control sample (HPMC/PVDF case) assuming all the three composites have the same specific heat capacity and cross-sectional area (Equation S1). The details about color ratio pyrometry are found in our previous studies [29,30]. Briefly, three-channel intensity (red, green, blue) ratios are extracted from a color camera. These data are processed using a house-built MATLAB routine and demosaiced for the camera's Bayer filter using standard MATLAB algorithms. The system was calibrated with a blackbody source (Mikron, Oriol), and the corresponding flame temperature maps were output and reported. The estimated temperature uncertainty is ≈ 200 – 300 K. The summary of all the samples is shown in Fig. S7.

3. Results and discussion

3.1. Enhanced energy release rate

We produced composite specimens containing 90wt% nanothermite and 10% PPC binder using a direct-ink-writing process and demonstrate a $> 15\text{X}$ energy release rate compared to a conventional polymer binder mixture (hydroxypropyl methylcellulose/polyvinylidene fluoride, HPMC/PVDF). High-speed microscopic imaging during combustion reveals a much thinner flame front (1/6) and lower-molecular-weight combustion products with PPC, confirming our hypothesis of decreased sintering. Fast-heating Time-of-Flight Mass Spectrometry further confirms that the unzipping polymer decomposes into volatiles at a relatively low temperature, which significantly reduces the sintering of Al NPs.

In this study, Al/CuO is chosen as it is one of the most studied fuel/oxidizer combinations [1–15] and PPC ($M_w \approx 196$ kDa) is chosen as an unzipping, gas-generating polymer binder. The choice of PPC is predicated on prior work that shows that depolymerization predominantly occurs through an unzipping mechanism to release propylene carbonate and carbon dioxide at temperatures near 250°C , thus below the ignition threshold for the fuel [31]. While other unzipping polymers are known, polymers that undergo chain-unzipping depolymerization via radical intermediates (like polymethyl methacrylate, PMMA, and polystyrene, PS) tend to leave behind char, presumably because they crosslink. PPC is considered to depolymerize by chain-unzipping mechanisms that do not involve radical intermediates, resulting in better-behaved outcomes (no char, only forms monomer) when depolymerizing from condensed (neat) neat phases. The other thing to note is that the temperature at which chain unzipping begins for PMMA [32] and PS [33] is considerably higher than PPC. The PPC used in this study contains 1 wt% photoacid generator (PAG) catalyst [34], which could be photolytically activated with ultraviolet (UV) irradiation under standard ambient conditions or thermally activated at temperatures as low as $\approx 180^\circ\text{C}$ [34,35], which could in principle be used to modulate the flame with contactless pre-processing approaches [36]. For the control, we used a previously developed

90 wt% Al/CuO loading ink formulation based on a polymer hybrid (1:1 by mass) of HPMC (M_w 86 kDa) and poly(vinylidene fluoride) (PVDF, M_w 534 kDa) [17,25]. HPMC gels upon heating via hydrophobic interactions and crosslinks [17], while PVDF is used as an energetic binder that can increase the ignitability of the composite [32–35,37–40]. In contrast, PPC is a thermoplastic that solidifies upon evaporation of the ink solvent dimethylformamide (DMF), as shown in Fig. S1. This behavior enables us to form free-standing composite sticks of 90 wt% Al and CuO NPs with only ≈ 10 wt% polymers.

The printed sticks (15 layers) show smooth, crack-free surfaces, (Fig. S1) with a dense packing. The density of the composites is determined by combining the cross-sectional area, length, and mass of the specimens [27,28]. The resulting value of $\approx 1.6 \text{ g}/\text{cm}^3$ approaches the theoretical packing density of NPs' aggregates (40%) [41,42], further confirming the dense packing of NPs in these printed stick composites. SEM cross-sections of the printed sticks in Fig. S1 also reveal close packing of these NPs but microscale aggregates of the Al (≈ 80 nm) and CuO (≈ 40 nm) NPs are present (Fig. S1). As shown in the low and higher magnification SEM images in Fig. S2, all three Al/CuO composite sticks have similar morphology, density, and NPs dispersion.

Typical flame propagation snapshots (from left to right) of the composite sticks along with the flame temperature maps are shown in Figs. 2a (PPC) and 2b (HPMC/PVDF). All combustion tests were conducted in 1 atm argon to exclude additional oxygen from air. The flame fronts proceed steadily for both samples and demonstrate a stable linear burn rate. The first and most important difference is that Al/CuO with PPC propagates at ≈ 40 cm/s, which is $\approx 13\text{X}$ faster than with HPMC/PVDF (≈ 3 cm/s). The flame temperature was obtained using an RGB color-ratio-based pyrometry technique [29,30], and the detailed time-resolved profiles are shown in Figs. 2c and 2d. The combustion of Al/CuO composite sticks with PPC (Fig. 2a and 2c) show a much larger and hotter exhaust flame with an average flame temperature of ≈ 3500 K. The flame temperature is ≈ 700 K lower than the control sample shown in Fig. 2b and 2d. The difference in flame temperatures indicates a large amount of hot gas/particle generation during PPC decomposition. The flame temperature of PPC-based composite (≈ 3500 K) is higher than the adiabatic flame temperature of Al/CuO (≈ 2840 K), which was also previously reported in Al/CuO nanolaminates [43]. This "super-adiabatic" discrete combustion arises in conditions where the chemistry is much faster than the heat dissipation and has been rigorously reviewed [44].

A comparison of the combustion performance by measuring the burn rate, flame temperature, ignition temperature, and energy release rate of the different composites is summarized in Fig. 3 (more details in supporting videos). The composites with PPC burn at a speed of ≈ 40 cm/s, which is $> 13\text{X}$ higher than the HPMC/PVDF case (Fig. 3a). Assuming the cross-sectional area and the heat capacity of each composite are roughly the same [27,28], the burn rate, density, and flame temperature are combined to obtain the relative energy release rate based on Equation S1. The composite with PPC binder shows a remarkable $> 15\text{X}$ energy release rate compared to the HPMC/PVDF binder (Fig. 3b). In contrast, both composites have similar ignition temperatures of $\approx 700^\circ\text{C}$, which is slightly higher than the melting point of Al ($\approx 660^\circ\text{C}$), and on par with the ignition temperature measured for the neat Al/CuO powder. This implies that any heat and gas released from the early decomposition of the polymers did not influence the ignition of Al/CuO chemically.

A complete understanding of the utility of unzipping polymers would also require an assessment of the mechanical properties [45,46], however, in our case for comparison purposes, both Al/CuO/HPMC/PVDF and Al/CuO/PPC composite (10% polymer) sticks have reasonable mechanical integrity. Despite the high heat

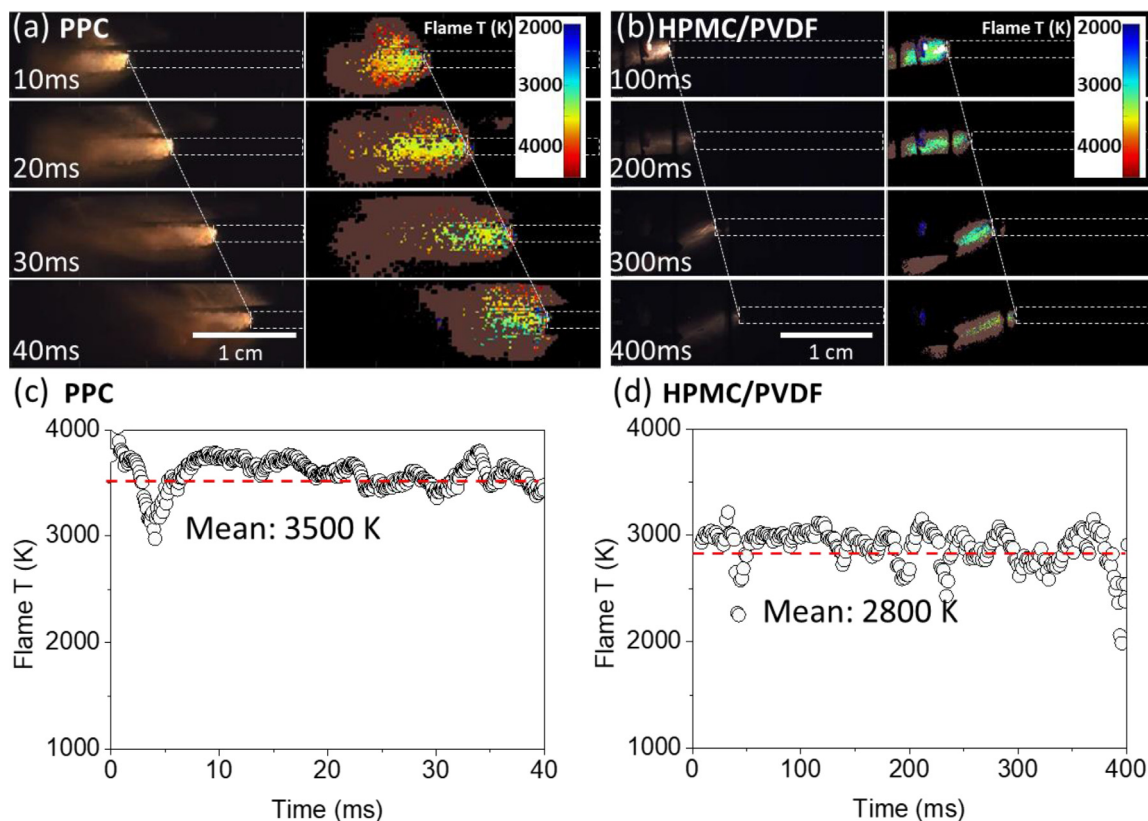


Fig. 2. Typical temporal burning snapshots, corresponding temperature maps (a, and b); time-resolved temperature profiles (c and d) of 90 wt% Al/CuO particle loading composites with PPC (a, and c) and HPMC/PVDF (b, and d).

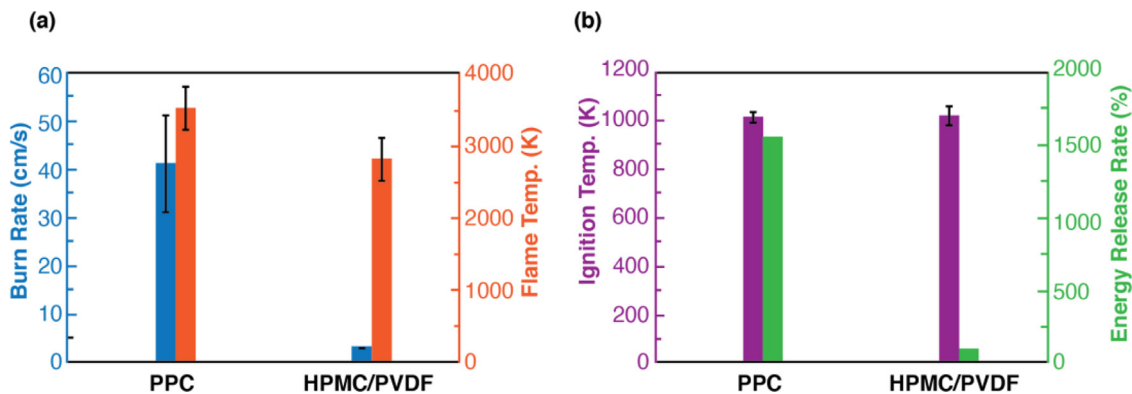


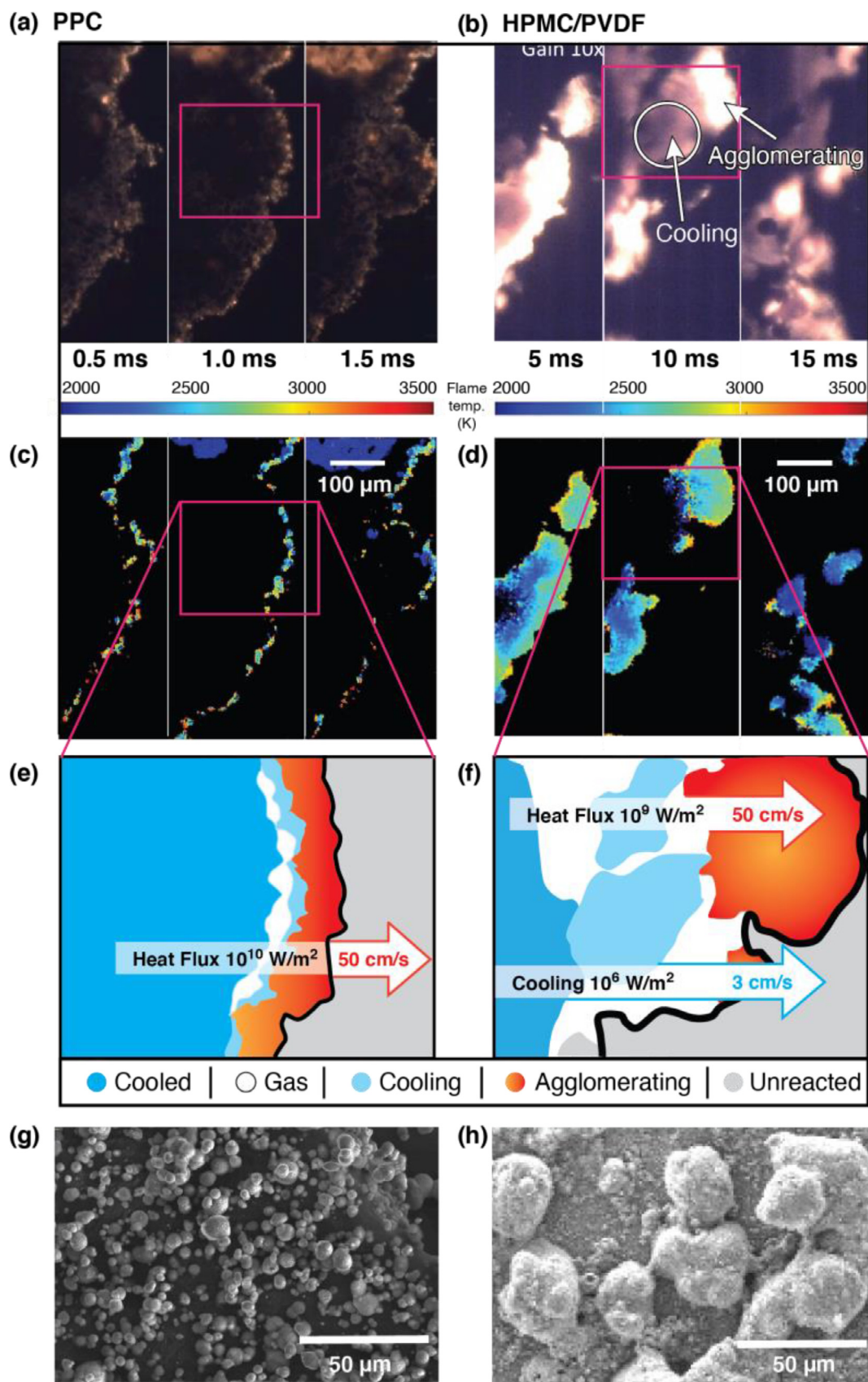
Fig. 3. The burn rate and flame temperature (a), ignition temperature, and energy release rate (b) of 90 wt.% particle loading Al/CuO composites with PPC and HPMC/PVDF.

fluxes [47–49], we see no issues related to mechanical integrity that would for the purposes of our comparison and demonstration of unzipping.

3.2. Thinner flame front and reduced agglomerations

To explore further the big difference between the two polymer systems, we zoom into the flame, to observe in greater detail what might be occurring on a flame-front scale. As previously mentioned, upon melting, NPs agglomerate/sinter into >1 μm scale particles during combustion, increasing the effective burning particle size by greater than 20X and significantly influencing the energy release rate [1–15]. To assess if the unzipping impacted sintering, and its relationship to a ≈ 15X increase in propagation, we employ microscopic imaging with a spatial and temporal resolution of ~μm and ~μs [27,28]. Typical snapshots with temper-

ature maps of the flame fronts are shown in Fig. 4a-4d, for the Al/CuO with PPC and HPMC/PVDF, respectively. The flame front for PPC composite is much thinner, and more continuous compared to HPMC/PVDF composite. Specifically, the thickness of the flame front for PPC is only ≈5–10 μm, which is about 10% of the thickness of the control. Fig. 4 and the supporting videos collectively suggest that the flame front consists of agglomerations of NPs with sizes that are similar to the thickness of the flame front. With HPMC/PVDF, as we have previously [17,25] and schematically show in Fig. 4f, the discontinuous flame front suggests an inhomogeneous reaction with heat fluxes during sintering (10⁹ W/m²) and cooling (10⁶ W/m²), supporting two different local (microscopic) propagating speeds of ≈50 cm/s and ≈3 cm/s, respectively. The overall macroscopic burn rate (≈3 cm/s) is limited by the slow step of cooling. By contrast, the flame front with PPC (Fig. 4e) is continuous, consisting of smaller particles with a ≈ 10X higher



9

Fig. 4. Typical microscopic snapshots (a, and b), corresponding flame temperature map (c, and d) and schematic showing (e, and f) the flame fronts of 90% particle loading Al/CuO composites with PPC and HPMC/PVDF. SEM images and size distribution (g, and h) of combustion products from Al/CuO with PPC and HPMC/PVDF. Note: more details about microscopic videos and combustion products SEM images are included in the supporting information.

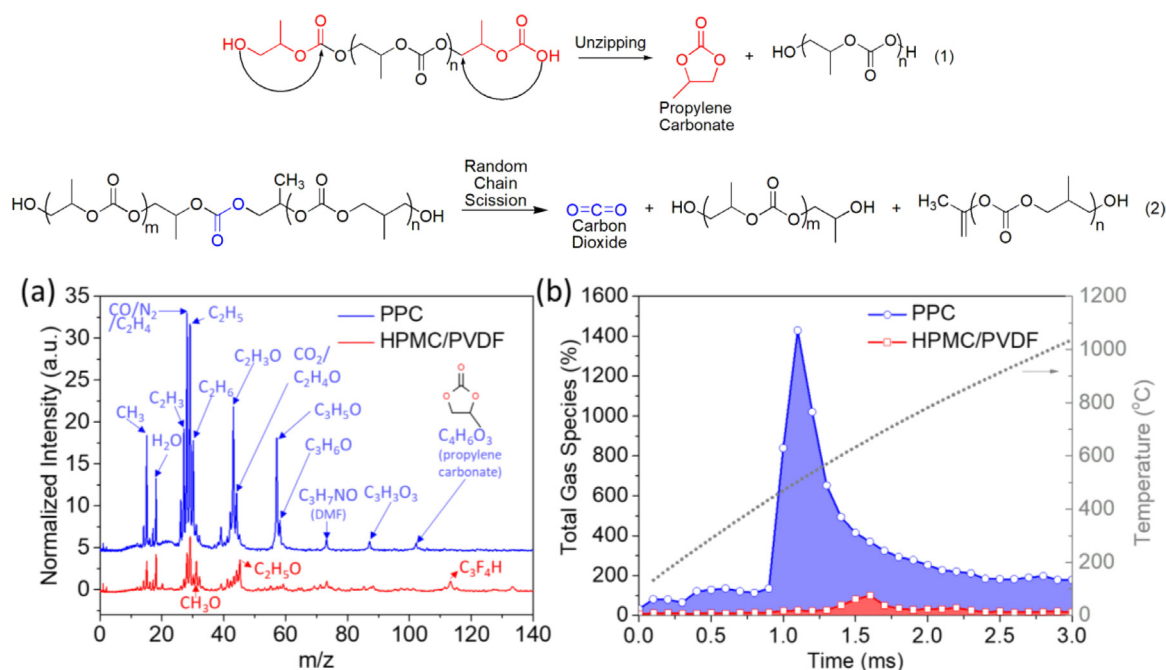


Fig. 5. T-Jump mass spectrum results of PPC and HPMC/PVDF (a); temporally integrated T-Jump mass spectra (b); temporal total gas release showing lower release temperature and significantly enhanced gas release for PPC. Note: (b) is a sum of top-10 gas species in (a). More details are in Fig. S5.

heat flux of $\approx 10^{10}$ W/m², which significantly enhances macroscopic flame propagating velocity to ≈ 50 cm/s (more details are in supporting videos). Consistent with the flame temperatures shown in Fig. 3a, the flame front of the PPC case shows higher temperatures (more yellow/red, less blue) compared to that of HPMC/PVDF. The post-combustion product SEM images (Fig. 4g and 4h) and size distribution (Fig. S3) confirm much smaller ejected particles for the PPC composite (≈ 4 μ m) compared to the HPMC/PVDF case (mean: ≈ 32 μ m). The microscopic high-speed videos and corresponding time-resolved temperature maps of the free-standing composite sticks further confirm that significantly smaller particles are produced and ejected from the burning surfaces (see supporting videos) from PPC compared to HPMC/PVDF.

3.3. Unzipping polymer promotes higher gas generation

We now turn our attention to the original premise, that the unzipping polymer acts as an efficient gas generator. PPC and HPMC/PVDF were coated on a thin (70 μ m) joule-heated platinum wire to study decomposition at a heating rate of $\approx 4 \times 10^5$ K·s⁻¹. The T-jump wire is coupled to a time-of-flight mass spectrometer capable of acquiring complete spectra at 10,000 Hz [26]. Fig. 5a shows mass spectra for the two cases and clearly indicates that PPC releases a significantly high amount of gas-phase species (time-resolved spectra in Fig. S4). Integrating the spectral peaks enables us to quantify the relative amount of gas and is presented as a sum total of gas produced as a function of molecular mass. Fig. 5b shows a 14X increase in gas production for PPC compared to HPMC/PVDF.

This is not surprising since PVDF contains no oxygen and leaves a significant amount of solid carbon residue upon decomposition (see oxygen balance calculations in Table S1). In contrast, PPC depolymerizes into gaseous monomers ($m/z = 102$, C₄H₆O₃) at a temperature as low as 350 °C (Fig. S5). These gaseous monomers (≈ 350 °C) further decompose into lighter species (Fig. S5) and peak at ≈ 500 °C (Fig. 5b); i.e., below the Al melting point (660 °C). This low-temperature gas decomposition should eject the NPs from the burning surface and minimize agglomerating/sintering (schemati-

cally shown in Fig. 1). On the other hand, half of the gas generation from HPMC/PVDF is $m/z > 60$ (Fig. 5a) and maximizes at a higher temperature at ≈ 650 °C (Fig. 5b) and very near the Al melting point where sintering is expected to be severe.

The thermal decomposition of PPC primarily occurs via two mechanisms: (i) polymer unzipping (Equation 1), and (ii) random chain scission (Equation 2) [33,34,50,51]. In this study, it is notable that there is a weak peak for CO₂ ($m/z = 44$) release at an earlier temperature of ≈ 300 °C (Fig. S5), which is attributed to random chain scission of PPC (Equation 2) [33,34,50,51]. The most prominent species detected are propylene carbonate ($m/z = 102$) and its fragments, indicating that unzipping (Equation 1) is the primary pathway [33,34,50,51].

We note finally that the integrated mass spectra show gas release ≈ 14 X higher, this corresponds remarkably close to the ≈ 15 X increase in burn rate and further evidence that unzipping is directly related to the enhanced energy release rate.

4. Conclusion

In summary, we demonstrate that using a polymer binder (PPC) that undergoes sequential unzipping to generate low-molecular-weight fragments results in propagation velocities of a nanoparticle fuel/oxidizer composite that are significantly enhanced. For the example of Al/CuO composites, energy delivery rates of 15 times higher than our previously developed hybrid polymer thermite composites. The flame temperature of PPC-based Al/CuO is also ≈ 700 K higher than that of the HPMC/PVDF case. We found that the burning of PPC-based Al/CuO composites has a flame front consisting of small agglomerations with a thickness ≈ 5 –10 μ m, which is $\approx 10\%$ of that previously observed for the HPMC/PVDF case. T-Jump mass spectrometry shows that upon fast heating, PPC depolymerizes to deliver a > 14 X increase in small-molecular-weight gaseous products, which significantly reduces NP agglomeration/sintering and dramatically enhances flame propagation and energy release rate. The results of the work are thus consistent with the original hypothesis as presented in Fig. 1. The results point to developing polymer systems that employ unzipping to

more efficiently use heat feedback to locally drive endothermic depolymerization, with large monomer production leading to reduced sintering of the metallic fuel and presumably a more complete combustion.

Supporting Information

Supporting Information is available from Elsevier or from the author.

Supporting macroscopic and microscopic combustion videos of the free-standing Al/CuO composite sticks with 10 wt% HPMC/PVDF, 10 wt% neat PPC, and 10 wt% PPC (1% PAG), respectively. Supporting microscopic combustion videos through the back of glass slides: Al/CuO composites with 10 wt% HPMC/PVDF and 10 wt% as received PPC, respectively. Low and higher magnification cross-sectional SEM images of the printed composite sticks, SEM/EDS and size distributions of the combustion products, burn rates, flame temperatures and energy release rate of all the printed samples: Al/CuO composite sticks with 10 wt% HPMC/PVDF, 10 wt% PPC (1% PAG), and 10 wt% neat PPC.

Declaration of Competing Interest

On behalf of all the authors, we declare no conflict of interest. This work is original and has not been considered for publication elsewhere.

Acknowledgements

We gratefully acknowledge support from ONR. We also thank the CFAMM at the University of California, Riverside, for their microscopy support.

Supplementary materials

Supplementary material associated with this article can be found, in the online version, at doi:[10.1016/j.combustflame.2022.112242](https://doi.org/10.1016/j.combustflame.2022.112242).

References

- [1] E.L. Dreizin, Metal-based reactive nanomaterials, *Prog. Energ. Combust.* 35 (2009) 141–167.
- [2] R.A. Yetter, Progress towards nanoengineered energetic materials, *Proc. Combust. Inst.* 38 (2021) 57–81.
- [3] J. Yu, Y. Wang, W. Wen, D. Yang, B. Huang, J. Li, K. Wu, Aluminothermal reaction approach for micro-/nanofabrications: syntheses of In_2O_3 micro-/nanostructures and InN octahedral nanoshells, *Adv. Mater.* 22 (2010) 1479–1483.
- [4] J.I. Gransden, M.J. Taylor, Study of confined pyrotechnic compositions for medium/large calibre gun igniter applications, *Propellants Explos. Pyrotech.* 32 (2007) 435–446.
- [5] S. Iyer, N. Slagg, Energetic materials, *Adv. Mater.* 2 (1990) 174–179.
- [6] A. Prakash, A.V. McCormick, M.R. Zachariah, Synthesis and reactivity of a super-reactive metastable intermolecular composite formulation of Al/ KMnO_4 , *Adv. Mater.* 17 (2005) 900–903.
- [7] S.H. Kim, M.R. Zachariah, Enhancing the rate of energy release from nanoenergetic materials by electrostatically enhanced assembly, *Adv. Mater.* 16 (2004) 1821–1825.
- [8] M. Comet, C. Martin, M. Klaumünzer, F. Schnell, D. Spitzer, Energetic nanocomposites for detonation initiation in high explosives without primary explosives, *Appl. Phys. Lett.* 107 (2015) 243108.
- [9] N.H. Yen, L.Y. Wang, Reactive metals in explosives, *Propellants Explos. Pyrotech.* 37 (2012) 143–155.
- [10] Y. Zhu, X. Zhou, J. Xu, X. Ma, Y. Ye, G. Yang, K. Zhang, In situ preparation of explosive embedded CuO/Al/CL20 nanoenergetic composite with enhanced reactivity, *Chem. Eng. J.* 354 (2018) 885–895.
- [11] E. Lafontaine, M. Comet, *Nanothermites*, ISTE Editions Ltd, London, UK, 2016.
- [12] W. He, P. Liu, G. He, M. Gozin, Q. Yan, Highly reactive metastable intermixed composites (MICs): preparation and characterization, *Adv. Mater.* 30 (2018) 1706293.
- [13] P. Chakraborty, M.R. Zachariah, Do nanoenergetic particles remain nano-sized during combustion? *Combust. Flame* 161 (2014) 1408–1416.
- [14] H. Wang, G. Jian, G.C. Egan, M.R. Zachariah, Assembly and reactive properties of Al/CuO based nanothermite microparticles, *Combust. Flame* 161 (2014) 2203–2208.
- [15] H. Wang, R.J. Jacob, J.B. DeLisio, M.R. Zachariah, Assembly and encapsulation of aluminum NP's within AP/NC matrix and their reactive properties, *Combust. Flame* 180 (2017) 175–183.
- [16] M.S. McClain, I.E. Gunduz, S.F. Son, Additive manufacturing of ammonium perchlorate composite propellant with high solids loadings, *P. Combust. Inst* 37 (2019) 3135–3142.
- [17] H. Wang, J. Shen, D.J. Kline, N. Eckman, N.R. Agrawal, T. Wu, P. Wang, M.R. Zachariah, Direct writing of a 90 wt% particle loading nanothermite, *Adv. Mater.* 31 (2019) 1806575.
- [18] N.V. Muravyev, K.A. Monogarov, U. Schaller, I.V. Fomenkov, A.N. Pivkina, Progress in additive manufacturing of energetic materials: creating the reactive microstructures with high potential of applications, *Propellants Explos. Pyrotech.* 44 (2019) 941–969.
- [19] W. Yang, M. Li, M. Xu, R. Hu, L. Zheng, Study of photocurable energetic resin based propellants fabricated by 3D printing, *Mater. Des.* 207 (2021) 109891.
- [20] Y. Mao, L. Zhong, X. Zhou, D. Zheng, X. Zhang, T. Duan, F. Nie, B. Gao, D. Wang, 3D printing of micro-architected Al/CuO-based nanothermite for enhanced combustion performance, *Adv. Eng. Mater.* 21 (2019) 1900825.
- [21] J. Shen, H. Wang, D.J. Kline, Y. Yang, X. Wang, M. Rehwoldt, T. Wu, S. Holdren, M.R. Zachariah, Combustion of 3D printed 90 wt% loading reinforced nanothermite, *Combust. Flame* 215 (2020) 86–92.
- [22] E.R. Wainwright, K.T. Sullivan, M.D. Grapes, Designer direct ink write 3D-Printed thermites with tunable energy release rates, *Adv. Eng. Mater.* 22 (2020) 1901196.
- [23] S.Q. Arlington, S.C. Barron, J.B. DeLisio, J.C. Rodriguez, S. Vummidi Lakshman, T.P. Weihs, G.M. Fritz, Multifunctional reactive nanocomposites via direct ink writing, *Adv. Mater. Technol.* 6 (2021) 2001115.
- [24] J.A. Kaitz, O.P. Lee, J.S. Moore, Depolymerizable polymers: preparation, applications, and future outlook, *MRS Commun* 5 (2015) 191–204.
- [25] H. Wang, D.J. Kline, M.R. Zachariah, In-operando high-speed microscopy and thermometry of reaction propagation and sintering in a nanocomposite, *Nat. Commun.* 10 (2019) 1–8.
- [26] L. Zhou, N. Piekil, S. Chowdhury, M.R. Zachariah, T-Jump/time-of-flight mass spectrometry for time-resolved analysis of energetic materials, *Rapid Commun. Mass Spectrom* 23 (2009) 194–202.
- [27] H. Wang, D.J. Kline, P. Biswas, M.R. Zachariah, Connecting agglomeration and burn rate in a thermite reaction: role of oxidizer morphology, *Combust. Flame* 231 (2021) 111492.
- [28] H. Wang, D.J. Kline, M.C. Rehwoldt, M.R. Zachariah, Carbon fibers enhance the propagation of high loading Nanothermites, *Situ Observation of Microscopic Combustion*, *ACS Appl. Mater. Interfaces* 13 (2021) 30504–30511.
- [29] R.J. Jacob, D.J. Kline, M.R. Zachariah, High speed 2-dimensional temperature measurements of nanothermite composites: probing thermal vs. gas generation effects, *J. Appl. Phys.* 123 (2018) 115902.
- [30] D.J. Kline, M.C. Rehwoldt, J.B. DeLisio, S.C. Barron, H. Wang, Z. Alibay, J.C. Rodriguez, G.M. Fritz, M.R. Zachariah, In-operando thermophysical properties and kinetics measurements of Al-Zr-C composites, *Combust. Flame* 228 (2021) 250–258.
- [31] X.H. Li, Y.Z. Meng, Q. Zhu, S.C. Tjong, Thermal decomposition characteristics of poly (propylene carbonate) using TG/IR and Py-GC/MS techniques, *Polym. Degrad. Stab.* 81 (2003) 157–165.
- [32] O.P. Korobeinichev, A.A. Paletsky, M.B. Gonchikzhapov, R.K. Glaznev, I.E. Gerasimov, Y.K. Naganovsky, I.K. Shundrina, A.Y. Snegirev, R. Vinu, Kinetics of thermal decomposition of PMMA at different heating rates and in a wide temperature range, *Thermochim. Acta.* 671 (2019) 17–25.
- [33] T. Faravelli, M. Pinciroli, F. Pisano, G. Bozzano, M. Dente, E. Ranzi, Thermal degradation of polystyrene, *J. Anal. Appl. Pyrolysis* 60 (2001) 103–121.
- [34] M. Garg, H.E. Aw, X. Zhang, P.J. Centellas, L.M. Dean, E.M. Lloyd, I.D. Robertson, Y. Liu, M. Yourdkhani, J.S. Moore JS, P.H. Geubelle, Rapid synchronized fabrication of vascularized thermosets and composites, *Nat. Commun.* 12 (2021) 1–9.
- [35] T.J. Spencer, P.A. Kohl, Decomposition of poly (propylene carbonate) with UV sensitive iodonium salts, *Polym. Degrad. Stab.* 96 (2011) 686–702.
- [36] Z. Alibay, D.J. Kline, M.C. Rehwoldt, P. Biswas, S. Herrera, H. Wang, M.R. Zachariah, Mechanism of microwave-initiated ignition of sensitized energetic nanocomposites, *Chem. Eng. J.* 415 (2021) 128657.
- [37] E.C. Koch, *Metal-Fluorocarbon Based Energetic Materials*, Wiley-VCH Verlag GmbH & Co. KGaA, Weinheim, Germany, 2012.
- [38] K.S. Kappagantula, C. Farley, M.L. Pantoya, J. Horn, Tuning energetic material reactivity using surface functionalization of aluminum fuels, *J. Phys. Chem. C* 116 (2012) 24469.
- [39] S. Huang, S. Hong, Y. Su, Y. Jiang, S. Fukushima, T.M. Gill, N.E. Yilmaz, S. Tiwari, K.I. Nomura, R.K. Kalia, A. Nakano, Enhancing combustion performance of nano-Al/PVDF composites with β -PVDF, *Combust. Flame.* 219 (2020) 467–477.
- [40] K.E. Uhlenhake, D. Olsen, M. Gomez, M. Örnek, M. Zhou, S.F. Son, Photoflash and laser ignition of full density nano-aluminum PVDF films, *Combust. Flame* 233 (2021) 111570.
- [41] G.D. Scott, D.M. Kilgour, The density of random close packing of spheres, *J. Phys. D: Appl. Phys.* 2 (1969) 863.
- [42] C. Zangmeister, J. Radney, L.T. Dockery, J.T. Young, X. Ma, R. You, M.R. Zachariah, Packing density of rigid aggregates is independent of scale, *P.N.A.S* 111 (2014) 9037–9041.
- [43] H. Wang, B. Julien, D.J. Kline, Z. Alibay, M.C. Rehwoldt, C. Rossi, M.R. Zachariah,

- Probing the reaction zone of nanolaminates at $\sim \mu\text{s}$ time and $\sim \mu\text{m}$ spatial resolution, *J. Phys. Chem. C* 124 (2020) 13679–13687.
- [44] A.S. Mukasyan, A.S. Rogachev, Discrete reaction waves: gasless combustion of solid powder mixtures, *Prog. Energy Combust. Sci.* 34 (2008) 377–416.
- [45] G. Prasad, K. Kishore, V.P. Verneker, Effect of ageing on ballistic and mechanical properties of propellants having various oxidiser loadings, *Combust. Flame.* 37 (1980) 197–199.
- [46] T. Kumar, T.L. Jackson, Three-dimensional thermo-mechanical simulations of heterogeneous solid propellants, *Combust. Flame.* 233 (2021) 111590.
- [47] S. Brotman, D.R. Mehdi, C. Samuel, E. Alain, C. Rossi, A Benchmark Study of burning rate of selected thermites through an original gasless theoretical model, *Appl. Sci.* 14 (2021) 6553.
- [48] Wang H, B. Prithwish, D.J. Kline, M.R. Zachariah, Flame stand-off effects on propagation of 3D printed 94wt.% nanosized pyrolants loading composites, *Chem. Eng. J.* 434 (2022) 134487.
- [49] G. Egan, M.R. Zachariah, Commentary on heat transfer mechanisms controlling propagation in nanothermites, *Combust. Flame* 162 (2015) 2959–2961.
- [50] O. Phillips, J.M. Schwartz, P.A. Kohl, Thermal decomposition of poly (propylene carbonate): end-capping, additives, and solvent effects, *Polym. Degrad. Stab.* 125 (2016) 129–139.
- [51] edited by C. David, Thermal degradation of polymers, in: C.H. Bamford, C.F.H. Tipper (Eds.), *Comprehensive Chemical Kinetics Volume 14: Degradation of Polymers*, Elsevier Scientific Publishing Company, New York (1975), pp. 1–173. edited by.